

Theoretical Analysis of Diffusion Models for Radio Map Estimation with Ultra-low Sampling Rates

Zhiyuan Liu[✉], *Student Member, IEEE*, Qingyu Liu[✉], *Member, IEEE*, Shuhang Zhang[✉], *Member, IEEE*,
Hongliang Zhang[✉], *Member, IEEE*, Lingyang Song[✉], *Fellow, IEEE*

Abstract—Radio maps, which characterize the spatial distribution of radio frequency metrics such as received signal strength, are essential for a wide range of wireless applications. The problem of radio map estimation involves constructing a radio map from sparse sensor measurements at multiple locations. This problem is particularly challenging due to ultra-low sampling rates, where available sensor measurements are far fewer than the high resolution requirement of radio maps to be estimated. Recently, diffusion models have been increasingly adopted for this problem, yet its theoretical performance remains unexamined. This paper bridges this gap by formulating radio map estimation as a non-linear matrix completion problem. Based on this formulation, we first derive a theoretical lower bound on the minimum estimation error achievable by diffusion models, which is fundamentally governed by the discrepancy between the deployment distribution and the true underlying radio propagation law. We then extend this bound to incorporate the effect of sampling sparsity, capturing the additional error introduced by ultra-low sampling rates. Furthermore, we establish a critical sampling rate threshold necessary for diffusion models to achieve performance convergence. Finally, considering that the derived error bounds depend on certain information that is difficult to obtain in practice, we propose empirical approximations that are readily computable from observable data. Extensive simulations based on real-world traces demonstrate that these empirical formulas tightly approximate the theoretical error bounds, validating their effectiveness for practical deployment.

Index Terms—Radio map estimation, spectrum cartography, diffusion model, generative AI.

I. INTRODUCTION

A radio map characterizes key parameters of wireless communication channels, such as received signal strength (RSS), at every location of a geographical area of interest [1]. It can significantly enhance the performance of various wireless applications, by supporting dynamic spectrum access [2], efficient spectrum sharing [3], fingerprint-based localization [4], and intelligent interference management [5].

Zhiyuan Liu and Qingyu Liu are with the School of Electronic and Computer Engineering, Peking University Shenzhen Graduate School, Shenzhen, China, 518055; and with the Pengcheng Laboratory, Shenzhen, China, 518055 (e-mail: liuzhiyuan@stu.pku.edu.cn, qy.liu@pku.edu.cn).

Shuhang Zhang and Hongliang Zhang are with the State Key Laboratory of Photonics and Communications, Beijing, China, 100871; and with the School of Electronics, Peking University, Beijing, China, 100871 (email: zhangshuhang@pku.edu.cn, hongliang.zhang@pku.edu.cn).

Lingyang Song is with the State Key Laboratory of Photonics and Communications, Beijing, China, 100871; with the School of Electronics, Peking University, Beijing, China, 100871; with the School of Electronic and Computer Engineering, Peking University Shenzhen Graduate School, Shenzhen, China, 518055; and with the Pengcheng Laboratory, Shenzhen, China, 518055 (e-mail: lingyang.song@pku.edu.cn).

The radio map estimation problem, specifically the sampling-based radio map estimation problem, requires the construction of a radio map based on the limited number of radio samples collected by sensors sparsely distributed in the area, as well as certain prior information such as the layout of obstacles [6], [7], [8]. This problem is particularly challenging due to ultra-low sampling rates: The high cost of capable radio sensing hardware (e.g., even a low-end sensor like the Ettus USRP B200mini can cost over 1,000 USD [9]) severely limits the number of sensors that can be deployed in practice. Consequently, radio samples are ultra-sparse compared to the high resolution of radio maps to be estimated. An effective solution of radio map estimation must be able to achieve accurate estimations with ultra-low sampling rates, making efficient use of extremely limited radio samples.

Traditional radio map estimation approaches are based on physics modeling [10], [11], [12] or interpolation [13], [14], [15], which utilize mathematical and statistical methodologies for estimation. However, these methods often fail to construct high-quality radio maps for real-world environments that are dynamic and geographically complex. This is because they do not account for certain critical prior information, such as the layout of obstacles, which can impact radio signal propagation.

Recent advances in generative Artificial Intelligence (AI), especially diffusion models, lead to a significant shift in how radio maps can be estimated. There are increasingly works proposing diffusion-based algorithms for radio map estimation. For example, Liu *et al.* [9] designed a diffusion-based generative framework for fine-grained radio map estimation. Wang *et al.* [16] proposed a decoupled diffusion model with an adaptive fast Fourier transform module for radio map estimation. Luo *et al.* [17] introduced a conditional denoising diffusion probabilistic model for radio map estimation from sparse measurements and transmitter locations. Qiu *et al.* [18] developed a diffusion model for interpolating indoor path loss radio maps from a limited number of reference points.

Despite the increasingly number of research works in this area, almost all of them adhere to a common profile: they designed diffusion-based models and evaluated them with large-scale simulated data or small-scale real-world data. However, no theoretical analysis on the performance of the proposed algorithms has been carried out. To the best of our knowledge, the sole work addressing the theoretical performance of radio map estimation is by Romero *et al.* [19]. Their study first provides a theoretical analysis of the spatial variability of radio maps and then derives upper bounds for the estimation error of certain interpolation-based methods. However, the results

in [19] are limited to free-space propagation environments and are specific to interpolation-based techniques. As such, they are not applicable to practical, complex environments where factors such as obstacle layouts critically impact propagation. They cannot be extended to diffusion-based algorithms, either.

In this work, we present a theoretical foundation for radio map estimation by diffusion models. Leveraging information theory and data-driven methodologies, we establish performance bounds and convergence guarantees for diffusion-based radio map estimation models. Specifically, the main contributions of this paper are summarized as follows:

- We formulate the problem of radio map estimation by diffusion models as a non-linear matrix completion problem. Based on the formulation, we derive a theoretical lower bound for the minimum estimation error achievable by diffusion models. This bound is a function of the difference between the deployment distribution and the true underlying radio propagation law. It provides a fundamental metric for assessing the effectiveness of diffusion-based radio map estimation methods.
- We extend the above bound to incorporate the effect of sampling rate, yielding a generalized lower bound for the estimation error that captures both distributional mismatch and measurement sparsity. This result quantifies the performance degradation of diffusion models induced by ultra-low sampling rates, thereby characterizing a key practical challenge in accurate radio map estimation.
- Moreover, based on the generalized sampling-dependent bound, we identify a critical sampling rate threshold above which diffusion models can achieve performance convergence. This threshold offers theoretical guidance for sampling strategy design: below it, estimation quality improves substantially with increased sampling rates; above it, further sampling yields only marginal gains.
- Finally, considering that the derived error bounds depend on certain information that is difficult to obtain in practice, we derive empirical formulas that approximate the error bounds and are readily computable from observable data. Extensive simulations based on real-world traces demonstrate that these empirical formulas tightly approximate the theoretical error bounds, validating their utility for practical deployment.

The rest of the paper is organized as follows. In Section II, we introduce related works. In Section III, we illustrate the problem definition of radio map estimation. In Section IV, we present the necessary background on matrix completion. In Section V, we formulate the diffusion-based radio map estimation problem as a non-linear matrix completion problem. In Section VI, we provide a convergence analysis of diffusion models for radio map estimation. In Section VII, we derive theoretical lower bounds for radio map estimation errors by diffusion models. In Section VIII, we propose empirical formulas to approximate our theoretical error bounds. In Section IX, we evaluate the proposed empirical approximation formulas via extensive simulations. Finally, Section X concludes the paper.

II. RELATED WORK

The problem of radio map estimation can generally be classified into two categories: sampling-free problem and sampling-based problem. The sampling-free problem uses the information from the transmitters to estimate radio maps. Existing studies solving these problems include [10], [11], [12]. The sampling-free problem assumes knowledge of the information (e.g., number, locations, and transmitting power) of transmitters. This assumption may not hold in practice, where there often exist many transmitters unknown to users. In contrast, the sampling-based problem uses a limited number of radio samples collected by sensors sparsely distributed within the region of interest, as well as certain prior information like the layout of obstacles, to estimate radio maps. In this paper, we focus on the sampling-based radio map estimation problem. This problem is challenging because of ultra-low sampling rates: The high cost of capable radio sensing hardware severely limits the number of sensors that can be deployed in practice. Consequently, radio samples are ultra-sparse compared to the high resolution of radio maps to be estimated.

Traditional radio map estimation approaches are based on physics modeling or interpolation, which utilize mathematical and statistical methodologies for estimation. Well-known methods include Ordinary Kriging (OK) [15], Radial Basis functions (RBF) [13], and Nearest Neighbor (NN) [20]:

- OK: It uses semivariogram functions to describe the spatial autocorrelation and estimates the RSS values of unknown points by weighted average of the observed data of known points.
- RBF: By creating a network of basis functions around the known data points, it uses a linear combination of these basis functions to approximate the RSS values of unknown points.
- NN: It utilizes a limited set of known radio samples to estimate RSS values at unknown locations, relying on the nearest neighbor principle.

Other interpolation-based approaches include Spline [14] and Inverse Distance Weighting (IDW) [21]. However, these methods often fail to construct high-quality radio maps for real-world environments that are dynamic and geographically complex. This is because they rely on mathematical calculations and do not account for certain critical prior information, such as the layout of obstacles, which can significantly impact radio signal propagation.

Recent advances in generative AI lead to a significant shift in how radio maps can be estimated. There are increasingly works proposing generative AI-based algorithms for radio map estimation, surpassing traditional physics modeling-based or interpolation-based approaches. Well-known methods include CollaboRadio [22] and RME-GAN [23].

- CollaboRadio: It is a device-edge-cloud collaboration framework, with a UNet-based small model and a Transformer-based large model proposed.
- RME-GAN: It is a two-phase conditional Generative Adversarial Network (GAN) framework that integrates model-based interpolation and learning-based refinement for radio map estimation.

Other generative AI-based approaches include RadioMamba [24], TVR [25], and UniRM [26]. Among various generative AI methods, diffusion model, a flagship technique in modern generative AI, progressively adds and then reverses noise to learn complex data distributions. It has been successfully applied to radio map estimation, achieving superior performance. Well-known diffusion-based approaches include WiFi-Diffusion [9], RadioDiff [16], RM-Gen [17], IRDM [18].

- WiFi-Diffusion: It first uses a diffusion model to generate a candidate set of radio maps with diverse qualities, and then employs principles of radio propagation to identify the most accurate map.
- RadioDiff: It is a decoupled diffusion model with an adaptive fast Fourier transform module used for radio map estimation.
- RM-Gen: It is a conditional denoising diffusion probabilistic model that generates complete radio maps using sparse RSS fragments and transmitter locations, incorporating an environment-aware method for selecting critical data pieces.
- IRDM: It is a generative diffusion model designed for indoor radio map interpolation that recovers complete path loss maps from a limited number of reference points, using a multi-stage training strategy and online data augmentation.

For these diffusion-based radio map estimation studies, they all adhere to a common profile: they designed diffusion-based models and evaluated them with large-scale simulated data or small-scale real-world data. However, no theoretical analysis on the performance of the proposed algorithms has been carried out, leaving their generalization performance to unseen data unverified.

To the best of our knowledge, the sole work addressing the theoretical performance of radio map estimation is by Romero *et al.* [19]. Their study first provides a theoretical analysis of the spatial variability of radio maps and then derives upper bounds for the estimation error of certain interpolation-based methods. However, the results in [19] are limited to free-space propagation environments and are specific to interpolation-based techniques. As such, they are not applicable to practical, complex environments where factors such as obstacle layouts critically impact propagation. They cannot be extended to diffusion models, either.

III. PROBLEM DEFINITION: RADIO MAP ESTIMATION

Consider a two-dimensional (2D) region of interest $\mathcal{X} \subset \mathbb{R}^2$. A set $\mathcal{S} = \{1, 2, \dots, S\}$ of S sensors is deployed over \mathcal{X} , where each sensor $s \in \mathcal{S}$ is located at a distinct coordinate $x_s \in \mathcal{X}$. Each sensor s measures RSS r_s in a specific frequency band at its location x_s (it is assumed that fast-fading effects are averaged out through minor temporal or spatial variations during measurement). These radio samples (RSS measurements) $\{r_s, \forall s \in \mathcal{S}\}$ are reported to a fusion center, which may be, e.g., a base station or a cloud server, depending on the application.

Consider that the continuous space \mathcal{X} is discretized into an $m \times n$ grid. A radio map can be represented by an $m \times n$ matrix

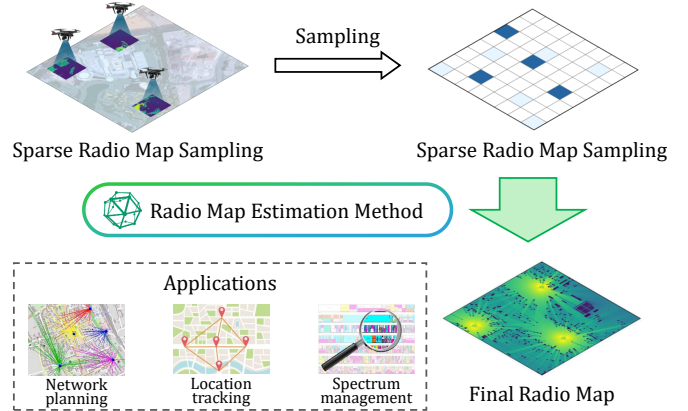


Fig. 1: An illustration of the radio map estimation problem.

\mathbf{M} , where its element at index (h, w) ($h \in \{0, 1, \dots, m-1\}$ and $w \in \{0, 1, \dots, n-1\}$) corresponds to the RSS at the respective spatial coordinate. Let Ψ denote an $m \times n$ binary mask, where its element at index (h, w) is 1 if a sensor is located at (h, w) ; otherwise, it is 0. Denote \odot as the Hadamard product. Then, the partial observation matrix $\mathbf{M} \odot \Psi$ yields an $m \times n$ matrix whose non-zero entries correspond to the RSS values measured by the sensors at their respective locations.

The problem of radio map estimation requires to use the sample collected by sensors sparsely distributed within \mathcal{X} , i.e., use the set $\{r_s, \forall s \in \mathcal{S}\}$, to estimate the radio map \mathbf{M} . Specifically, as depicted in Fig. 1, radio map estimation requires the fusion center to use the incomplete observations $\mathbf{M} \odot \Psi$ to estimate \mathbf{M} which presents the RSS at every location within the region \mathcal{X} .

IV. PRELIMINARIES: MATRIX COMPLETION

Our analysis of using diffusion models to solve the radio map estimation problem is based on a matrix completion-based formulation. In order to describe the formulation, it is necessary to first introduce matrix completion in this section.

The problem of matrix completion requires to recover missing entries in partially observed matrices [27]. It has been widely applied to numerous tasks, such as collaborative filtering [28], image recovery and inpainting [29], and classification [30].

A. Low-Rank Matrix Completion

A fundamental assumption underlying traditional matrix completion methods is that the target data matrix is low-rank. This low-rank property allows missing entries to be recovered by minimizing the matrix rank.

Specifically, theoretical studies have shown that, under certain constraints on the missing rate, matrix rank, and sampling scheme, missing entries in a low-rank matrix can be exactly recovered by addressing a rank minimization problem [31]. Mathematically, for a matrix $\mathbf{M}_{m \times n}$ and an observation position set Ω , define a sparse observation mask as

$$[\Psi]_{ij} = \begin{cases} 1 & \text{if } (i, j) \in \Omega \\ 0 & \text{otherwise.} \end{cases}$$

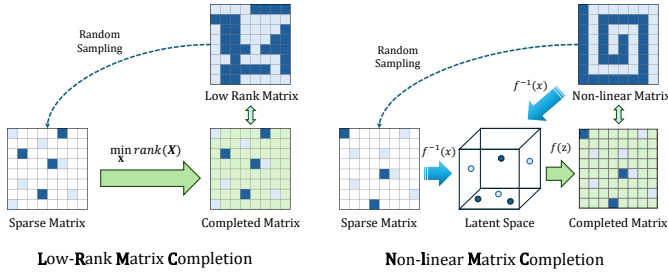


Fig. 2: An illustration of the matrix completion problem.

Then, for matrix \mathbf{X} to be recovered, the low-rank matrix completion problem can be formulated as:

$$\begin{aligned} & \min_{\mathbf{X}} \text{rank}(\mathbf{X}) \\ & \text{subject to } \mathbf{X} \odot \Psi = \mathbf{M} \odot \Psi. \end{aligned}$$

where $\mathbf{X}_{m \times n}$ is the decision variable.

B. Non-Linear Matrix Completion

Traditional matrix completion methods often fail to recover missing entries in partially observed matrices by minimizing the matrix rank when the matrix has a high rank. To address this and recover missing elements in high-rank matrices, non-linear matrix completion jointly optimizes both a non-linear mapping from the high-rank matrix to a low-dimensional latent space and the latent structure [32]. They assume that the data of the high-rank matrix is given by a non-linear latent variable model, and have proved that minimizing the latent space dimension can exactly solve the matrix completion problem.

Mathematically, let $f(\cdot)$ be a non-linear transformation that relates a low-dimensional latent space and the high-rank matrix. The non-linear matrix completion problem is:

$$\begin{aligned} & \min_{\mathbf{Z}} \dim(\mathbf{Z}) \\ & \text{subject to } \mathbf{X} = f(\mathbf{Z}), \mathbf{X} \odot \Psi = \mathbf{M} \odot \Psi. \end{aligned}$$

where \mathbf{Z} is the latent space variable.

For the above problem, let the sampling rate be $\rho = \frac{|\Omega|}{mn}$. A necessary condition for the problem to be solvable is [33]:

$$\text{rank}(\mathbf{Z}) \leq \rho \cdot \min(m, n). \quad (1)$$

Depending on the non-linear mapping model, existing approaches for non-linear matrix completion can be basically categorized into two categories, i.e., kernel trick approaches [32] and Deep Matrix Factorization (DMF) approaches [33].

Kernel Trick-Based Non-Linear Matrix Completion It maps the sparsely sampled matrix into a high-dimensional space using kernel methods, thereby constructing a high-dimensional yet low-rank matrix. Matrix completion is then performed in this high-dimensional space via low-rank matrix completion.

Specifically, to handle non-linearity, a non-linear function $\phi(\cdot)$ is defined to map X into a feature space \mathcal{F} : $\phi(\cdot) : \mathbb{R}^m \rightarrow \mathcal{F}^l$, where \mathcal{F} is an inner product space whose dimension l can be arbitrarily large or even infinite. Data in \mathcal{F} can then be

processed using linear techniques. The matrix formed by the data in the feature space is

$$W = \Phi(X) = [\phi(x_1), \phi(x_2), \dots, \phi(x_n)],$$

which is expected to be low-rank or approximately low-rank. This implies that in the high-dimensional feature space, W originates from a low-dimensional subspace and can be represented by a linear transformation of a small number of latent variables. This aligns with the situation in the input space, where X is redundant and can be expressed via a non-linear transformation $f(\cdot)$ of a small set of latent variables Z . Therefore, minimizing the rank of W is equivalent to minimizing the dimension of non-linear latent variables of X .

As a result, the missing entries of X can be recovered by solving the following problem:

$$\min_{\mathbf{X}} \text{rank}(W), \text{ s.t. } W = \Phi(X), \mathbf{X} \odot \Psi = \mathbf{M} \odot \Psi, (i, j) \in \Omega,$$

This problem is NP-hard but can be approximated as:

$$\min_{\mathbf{X}} \|W\|_{S_p}^p, \text{ s.t. } W = \Phi(X), \mathbf{X} \odot \Psi = \mathbf{M} \odot \Psi, (i, j) \in \Omega.$$

Here, the Schatten p -norm serves as a non-convex relaxation of the rank, and is defined as:

$$\|W\|_{S_p} = \left(\sum_{i=1}^{\min(n,l)} (\sigma_i(W))^p \right)^{1/p}.$$

Kernel trick-based non-linear matrix completion approaches are limited by their computational inefficiency and moderate reconstruction performance.

DMF-Based Non-Linear Matrix Completion It builds upon the non-linear latent variable model by constructing a deep-structured neural network. It takes low-dimensional unknown latent variables as input and partially observed variables as output. By simultaneously optimizing the latent variables and network parameters to minimize the reconstruction error of the observed entries, it recovers the missing ones. Compared to kernel trick-based approaches, DMF-based approaches have significantly lower computational complexities and are suitable for the completion of large-scale matrices. The formal expression of DMF-based non-linear matrix completion is:

$$\begin{aligned} & \min_{Z, f} \pi(f) + \frac{\beta}{2n} \|Z\|_F^2, \\ & \text{s.t. } [f(Z)]_{i,j} = X_{i,j}, (i, j) \in \Omega, \end{aligned}$$

where $\pi(f)$ denotes the penalty or constraint on $f(\cdot)$, and β is the regularization parameter for Z . Regularization of both $f(\cdot)$ and Z is necessary since there are infinitely many solutions of $f(\cdot)$ and Z that can reproduce the observed entries of X .

In practice, the observed entries of X are often contaminated by small noise, and it is impractical for $[f(Z)]_{i,j}$ to exactly equal $X_{i,j}$. It suffices to minimize the discrepancy between $[f(Z)]_{i,j}$ and $X_{i,j}$:

$$\min_{Z, f} \frac{1}{2n} \|\Psi \odot (X - f(Z))\|_F^2 + \frac{\beta}{2n} \|Z\|_F^2 + \lambda \pi(f).$$

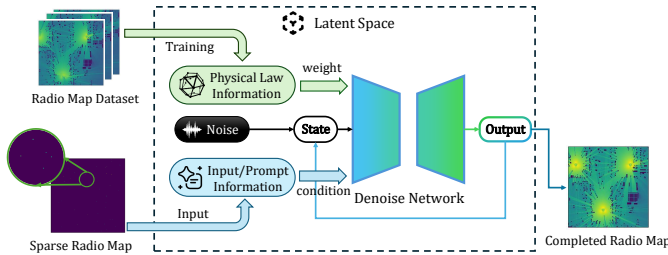


Fig. 3: An illustration of using diffusion models for radio map estimation.

where λ is a regularization parameter. The non-linear function can be approximated using a neural network:

$$\min_{\mathbf{Z}, \Theta} \frac{1}{2n} \sum_{i=1}^n \|\Psi_i \odot (x_i - g^{(K+1)}(g^{(K)}(\dots g^{(1)}(z_i, \Theta^{(1)}), \dots, \Theta^{(K)}), \Theta^{(K+1)}))\|^2 + \frac{\beta}{2n} \|\mathbf{Z}\|_F^2 + \frac{\lambda}{2} \sum_{j=1}^{K+1} \|W^{(j)}\|_F^2,$$

where $\Theta^{(j)} = (W^{(j)}, b^{(j)})$, $g^{(j)}(t, \Theta^{(j)}) = g^{(j)}(W^{(j)}t + b^{(j)})$, for $j = 1, 2, \dots, K+1$, and K is the number of hidden layers.

Although DMF-based methods offer theoretical advantages (e.g., guaranteed complete recovery above a certain sampling threshold), they remain limited when sampling falls below that threshold, where insufficient information prevents exact reconstruction. Furthermore, DMF differs fundamentally from typical deep learning models like CNNs used for image classification. CNNs are trained on massive image datasets to learn general feature extraction capabilities applicable to all images. In contrast, DMF aims to precisely capture the internal structure and patterns of a specific matrix. It is tailored only to that particular matrix and is not designed to generalize to other unrelated matrices.

V. MATRIX COMPLETION-BASED FORMULATION FOR DIFFUSION-BASED RADIO MAP ESTIMATION

Although standard non-linear matrix completion can take sparse sensor measurements into consideration, they fail to account for certain prior information that is critical for radio map estimation, e.g., well-established radio propagation principles. To address this limitation, we are motivated by Inductive Matrix Completion (IMC) [34], which utilizes side information to construct non-linear mappings. In this section, we thereby introduce a non-linear matrix completion formulation for the problem of using diffusion models to estimate radio maps.

A radio map is in fact a high-rank matrix of RSS values, derived from a latent and potentially unknown propagation law conditioned on environmental factors, such as building layouts and terrain, which influence signal behavior. As shown in Fig. 3, when a diffusion model is applied to radio map estimation, it learns the complex mapping from radio propagation law to RSS matrices during training, using a dataset that encodes the propagation law alongside ground-truth RSS matrices. This learning process is aligned intuitively with the problem of non-linear matrix completion.

Mathematically, let $\mathbf{M}_{m \times n}$ denote the target radio map to be estimated, and let $G_\theta(\cdot)$ represent a diffusion model parameterized by θ . Let \mathcal{P} be the underlying distribution of radio maps, governed by a latent and potentially unknown radio propagation law, and let \mathbf{Z} denote the input noise to the diffusion model. Given a binary observation mask Ψ indicating sensor locations, the problem of radio map estimation by diffusion models can be formulated as:

$$\min_{\theta, \mathbf{X}} \mathbf{W}(G_\theta, \mathcal{P}),$$

$$\text{subject to } \mathbf{X} = G_\theta(\mathbf{Z}; \mathbf{M} \odot \Psi), \mathbf{X} \odot \Psi = \mathbf{M} \odot \Psi. \quad (2)$$

where \mathbf{W} denotes the Wasserstein distance, which measures the similarity between different distributions. Specifically, for two probability measures $\mu, \nu \in P(\mathbb{R}^d)$,

$$\mathbf{W}(\mu, \nu) = \inf_{\gamma \in \Gamma(\mu, \nu)} \int_{\mathbb{R}^d \times \mathbb{R}^d} \|x - y\| d\gamma(x, y) \quad (3)$$

where $\Gamma(\mu, \nu)$ represents the set of all coupling measures with marginals μ and ν .

VI. CONVERGENCE ANALYSIS OF DIFFUSION MODELS FOR RADIO MAP ESTIMATION

Diffusion models address the radio map estimation problem by gradually injecting noise to smoothly transform the complex data distribution of radio propagation laws into a known prior distribution, and then reversing the process by gradually removing noise to reconstruct the data distribution from the prior. This idea aligns with the framework of Stochastic Differential Equations (SDEs), which is the basic mathematical paradigm of diffusion models [35]. In this section, we establish the convergence of the diffusion model for radio map estimation using the SDE optimization theory, providing a theoretical foundation for the analysis of the estimation errors of diffusion models in subsequent sections.

The objective of the diffusion model is to construct a diffusion process $\{\mathbf{x}(t)\}_{t=0}^T$, indexed by a continuous time variable $t \in [0, T]$, such that $\mathbf{x}(0) \sim p_0 = \mathcal{P}$ (the data distribution of radio propagation) and $\mathbf{x}(T) \sim p_T$ (a tractable prior distribution with a known analytic form). This diffusion process can be modeled as the solution to an Itô SDE:

$$d\mathbf{x} = \mathbf{f}(\mathbf{x}, t) dt + g(t) d\mathbf{w}, \quad (4)$$

where \mathbf{w} denotes the standard Wiener process (also known as Brownian motion), $\mathbf{f}(\cdot, t) : \mathbb{R}^d \rightarrow \mathbb{R}^d$ is a vector-valued function referred to as the drift coefficient of $\mathbf{x}(t)$, and $g(\cdot) : \mathbb{R} \rightarrow \mathbb{R}$ is a scalar function known as the diffusion coefficient of $\mathbf{x}(t)$. As long as these coefficients are globally Lipschitz continuous in both state and time, the SDE admits a unique strong solution [36].

Let $p_t(\mathbf{x})$ be the probability density of $\mathbf{x}(t)$, and $p_{st}(\mathbf{x}(t) | \mathbf{x}(s))$ be the transition kernel from $\mathbf{x}(s)$ to $\mathbf{x}(t)$ for $0 \leq s < t \leq T$. Typically, p_T is an unstructured prior that contains no information about p_0 , such as a Gaussian distribution with fixed mean and variance. By initializing from samples $\mathbf{x}(T) \sim p_T$ and reversing the diffusion process, we can obtain samples $\mathbf{x}(0) \sim p_0$. A seminal result by

Anderson [37] establishes that the reverse of a diffusion process is itself a diffusion process evolving backward in time, governed by the following reverse-time SDE:

$$d\mathbf{x} = [\mathbf{f}(\mathbf{x}, t) - g(t)^2 \nabla_{\mathbf{x}} \log p_t(\mathbf{x})] dt + g(t) d\bar{\mathbf{w}}, \quad (5)$$

where $\bar{\mathbf{w}}$ is a standard Wiener process when time flows backwards from T to 0, and dt represents an infinitesimal negative time step. Once the score $\nabla_{\mathbf{x}} \log p_t(\mathbf{x})$ of each marginal distribution is known for all t , the reverse diffusion process can be derived from Eq. (5) and simulated to draw samples from p_0 .

The score of a distribution can be estimated by training a score-based model on data samples using score matching [38]. To estimate $\nabla_{\mathbf{x}} \log p_t(\mathbf{x})$, one can train a time-dependent score-based model $\mathbf{s}_{\theta}(\mathbf{x}, t)$ via a continuous generalization of noise conditional score network (NCSN) training target [39], and evidence lower bound (ELBO) of denoising diffusion probabilistic models (DDPM) [40]:

$$\begin{aligned} \theta^* = \arg \min_{\theta} \mathbb{E}_t \{ & \lambda(t) \mathbb{E}_{\mathbf{x}(0)} \mathbb{E}_{\mathbf{x}(t)|\mathbf{x}(0)} [\| \mathbf{s}_{\theta}(\mathbf{x}(t), t) \\ & - \nabla_{\mathbf{x}(t)} \log p_{0t}(\mathbf{x}(t) | \mathbf{x}(0)) \|_2^2] \}. \end{aligned} \quad (6)$$

Here, $\lambda : [0, T] \rightarrow \mathbb{R}_{>0}$ is a positive weighting function, t is uniformly sampled over $[0, T]$, $\mathbf{x}(0) \sim p_0(\mathbf{x})$, and $\mathbf{x}(t) \sim p_{0t}(\mathbf{x}(t) | \mathbf{x}(0))$. Given sufficient data and model capacity, score matching guarantees that the optimal solution to Eq. (6), denoted as $\mathbf{s}_{\theta^*}(\mathbf{x}, t)$, equals to $\nabla_{\mathbf{x}} \log p_t(\mathbf{x})$ for almost all \mathbf{x} and t .

In practice, knowledge of the transition kernel $p_{0t}(\mathbf{x}(t) | \mathbf{x}(0))$ is typically required to efficiently optimize Eq. (6). When $\mathbf{f}(\cdot, t)$ is affine, this kernel is Gaussian with closed-form expressions for its mean and variance, obtainable via standard techniques. For instance, the perturbation kernels $\{p_{\alpha_i}(\mathbf{x} | \mathbf{x}_0)\}_{i=1}^N$ used in DDPM, one well-known diffusion model, correspond to the discrete Markov chain:

$$\mathbf{x}_i = \sqrt{1 - \beta_i} \mathbf{x}_{i-1} + \sqrt{\beta_i} \mathbf{z}_{i-1}, \quad i = 1, \dots, N. \quad (7)$$

In the limit as $N \rightarrow \infty$, this discrete process converges to the following SDE:

$$d\mathbf{x} = -\frac{1}{2} \beta(t) \mathbf{x} dt + \sqrt{\beta(t)} d\mathbf{w}. \quad (8)$$

To ensure that the above optimization process in Eq. (6) effectively solves the problem of radio map estimation formulated in Eq. (2), it is essential to establish the convergence of the diffusion model. Bortoli [41] have proved that if the following 4 assumptions hold:

- **A1.** The data distribution \mathcal{P} is supported on a compact set \mathcal{M} , and $0 \in \mathcal{M}$,
- **A2.** $t \mapsto \beta_t$ is continuous, non-decreasing, and there exists $\bar{\beta} > 0$ such that for any $t \in [0, T]$, $1/\bar{\beta} \leq \beta_t \leq \bar{\beta}$,
- **A3.** There exist $\mathbf{s} \in C([0, T] \times \mathbb{R}^d, \mathbb{R}^d)$ and $M \geq 0$ such that for any $t \in [0, T]$ and $x_t \in \mathbb{R}^d$,

$$\| \mathbf{s}(t, x_t) - \nabla \log p_t(x_t) \| \leq M(1 + \|x_t\|) / \sigma_t^2, \quad (9)$$

- **A4.** $\gamma_k \sup_{v \in [T-t_{k+1}, T-t_k]} \beta_v / \sigma_v^2 \leq \delta \leq 1/2$, for any $k \in \{0, \dots, K-1\}$,

and $T \geq 2\bar{\beta}(1 + \log(1 + \text{diam}(\mathcal{M})))$, $\gamma_K = \varepsilon$, and $\varepsilon, M, \delta \leq 1/32$, there exists $D_0 \geq 0$ such that

$$\begin{aligned} \mathbf{W}(G_{\theta}, \mathcal{P}) \leq D_0 (\exp[\kappa/\varepsilon] (M + \delta^{1/2}) / \varepsilon^2 \\ + \exp[\kappa/\varepsilon] \exp[-T/\bar{\beta}] + \varepsilon^{1/2}), \end{aligned} \quad (10)$$

where $\kappa = \text{diam}(\mathcal{M})^2(1 + \bar{\beta})/2$ and

$$D_0 = D(1 + \bar{\beta})^7(1 + d + \text{diam}(\mathcal{M})^4)(1 + \log(1 + \text{diam}(\mathcal{M}))), \quad (11)$$

where D is a constant, $\text{diam}(\mathcal{M})$ denotes the diameter of the manifold, defined as $\text{diam}(\mathcal{M}) = \sup\{\|x - y\| : x, y \in \mathcal{M}\}$, σ_t is the noise scale of the forward SDE in the diffusion process, and $\varepsilon > 0$ is a small hyperparameter.

For radio map estimation by diffusion models, **A1** holds because radio maps follow underlying radio propagation laws, even when these laws are not explicitly known. **A2** is satisfied in all scheduling schemes used in practice. The explosive behavior as $t \rightarrow 0$ considered in **A2** is properly accounted for in real-world implementations. **A3** and **A4** hold for the SDE. Consequently, the diffusion model is guaranteed to converge when applied to the problem of radio map estimation.

VII. THEORETICAL RADIO MAP ESTIMATION ERRORS OF DIFFUSION MODELS

In this section, we analyze the theoretical performance of diffusion models for radio map estimation. First, recognizing that any estimated radio map will inevitably deviate from the ground truth due to discrepancies between the deployment domain distribution and the true underlying radio propagation law, we derive a lower bound on the optimality gap (minimum estimation error) achievable by a diffusion model. Next, we extend this lower bound to take sampling rate into consideration, thereby capturing the additional error introduced by ultra-sparse sampling. Finally, we establish a sampling rate threshold above which the diffusion model achieves performance convergence.

A. Minimum Estimation Error

In the context of generative AI, deployment domain distribution refers to the data distribution encountered when a trained model is deployed in a real-world environment. For radio map estimation, variations in deployment scenarios can cause the deployment domain distribution to deviate from the true underlying radio propagation law. Let $\tilde{\mathcal{P}}$ denote the deployment domain distribution. Then, $\mathbf{W}(G_{\theta}, \tilde{\mathcal{P}})$ characterizes the minimum error E_{min} of using diffusion models for radio map estimation. According to the convergence theory of diffusion models, with a suitable estimator, the convergence effect can be related to the recovery effect measured by Mean Squared Error (MSE) [42], i.e., we can have:

$$E_{min} = \| \mathbf{X}_{max} - \tilde{\mathbf{M}} \|^2, \quad (12)$$

where \mathbf{X}_{max} is the best map (matrix) reconstructed by diffusion models, and $\tilde{\mathbf{M}}$ is the map (matrix) corresponding to the deployment domain distribution.

Based on the convergence theory of diffusion models [35], [41], which relates the Wasserstein distance to the convergence

effect, we derive the following theorem, which establishes the minimum estimation error achievable by diffusion models.

Theorem 1. *The minimum estimation error E_{\min} (defined in Eq. (12)) of using diffusion models for radio map estimation satisfies:*

$$E_{\min} = \mathcal{R}(\mathcal{P}, \tilde{\mathcal{P}}) \cdot \mathbf{W}(\mathcal{P}, \tilde{\mathcal{P}}) + \zeta, \quad (13)$$

where $\mathcal{R}(\mathcal{P}, \tilde{\mathcal{P}})$ is an influence factor related to the manifold geometry of distributions \mathcal{P} and $\tilde{\mathcal{P}}$, used to scale the distribution error to the specific data error and defined as:

$$\mathcal{R}(\mathcal{P}, \tilde{\mathcal{P}}) = C \cdot \left(\frac{\text{diam}(\mathcal{A}) + \text{diam}(\tilde{\mathcal{A}})}{2} \right) \cdot \left(1 + \log \left(1 + \mathbf{W}(\mathcal{P}, \tilde{\mathcal{P}}) \right) \right) \quad (14)$$

Here \mathcal{A} and $\tilde{\mathcal{A}}$ are the supporting manifolds of distributions \mathcal{P} and $\tilde{\mathcal{P}}$ respectively, $\text{diam}(\cdot)$ denotes the diameter of the manifold, and C is a constant related to the diffusion model parameters. ζ is an error term reflecting the approximation error between the diffusion model G_θ and the training distribution \mathcal{P} .

Proof: Consider the training distribution \mathcal{P} and the deployment distribution $\tilde{\mathcal{P}}$, supported on compact manifolds \mathcal{A} and $\tilde{\mathcal{A}}$ respectively. According to the triangle inequality property of the Wasserstein distance, we have:

$$|\mathbf{W}(G_\theta, \tilde{\mathcal{P}}) - \mathbf{W}(\mathcal{P}, \tilde{\mathcal{P}})| \leq \mathbf{W}(G_\theta, \mathcal{P}).$$

As a result, we have:

$$\mathbf{W}(G_\theta, \tilde{\mathcal{P}}) = \mathbf{W}(\mathcal{P}, \tilde{\mathcal{P}}) + \delta_w$$

where $\delta_w \in [-\mathbf{W}(G_\theta, \mathcal{P}), \mathbf{W}(G_\theta, \mathcal{P})]$ is a random variable, whose absolute value decreases with convergence.

Thus, due to the influence of diffusion model convergence, the theoretical minimum error E_{\min} is primarily determined by the inter-distribution distance $\mathbf{W}(\mathcal{P}, \tilde{\mathcal{P}})$, but needs to be modulated by the manifold geometry to map from the distribution to the specific sampling error. Therefore, we establish:

$$E_{\min} = \mathcal{R}(\mathcal{P}, \tilde{\mathcal{P}}) \cdot \mathbf{W}(\mathcal{P}, \tilde{\mathcal{P}}) + \zeta$$

where $\mathcal{R}(\mathcal{P}, \tilde{\mathcal{P}})$ is an influence factor related to the manifold geometry of distributions \mathcal{P} and $\tilde{\mathcal{P}}$, and ζ represents the contribution of the generative model approximation error.

According to the convergence theory of diffusion models under the manifold assumption [35], [41], the Wasserstein distance between the generative distribution G_θ and the target distribution \mathcal{P} satisfies:

$$\mathbf{W}(G_\theta, \mathcal{P}) \leq D_0 (\exp[\kappa/\varepsilon] (\mathbb{M} + \delta^{1/2}) / \varepsilon^2 + \exp[\kappa/\varepsilon] \exp[-T/\bar{\beta}] + \varepsilon^{1/2})$$

where the constant D_0 depends on the manifold diameter $\text{diam}(\mathcal{A})$, dimension d , and diffusion parameters $\bar{\beta}$.

According to the convergence analysis of diffusion models on manifolds, the constant D_0 has the form [41]:

$$D_0 = D(1 + \bar{\beta})^7 (1 + d + \text{diam}(\mathcal{A})^4) (1 + \log(1 + \text{diam}(\mathcal{A})))$$

This indicates that the convergence rate is closely related to the manifold diameter. For the distribution shift scenario, we need

to consider the geometric characteristics of both the source manifold \mathcal{A} and the target manifold $\tilde{\mathcal{A}}$, so we can define the geometric factor:

$$\mathcal{R}(\mathcal{P}, \tilde{\mathcal{P}}) = C \cdot \left(\frac{\text{diam}(\mathcal{A}) + \text{diam}(\tilde{\mathcal{A}})}{2} \right) \cdot \left(1 + \log \left(1 + \mathbf{W}(\mathcal{P}, \tilde{\mathcal{P}}) \right) \right)$$

where C incorporates constant terms such as dimension d and diffusion parameters $\bar{\beta}$. The logarithmic term $1 + \log(1 + \mathbf{W}(\mathcal{P}, \tilde{\mathcal{P}}))$ ensures that the geometric factor does not shrink excessively in cases of small shifts.

According to diffusion model convergence theory, the optimal performance of the generator is limited by its fit to the training distribution:

$$\mathbf{W}(G_\theta^*, \mathcal{P}) \leq \epsilon_{\text{opt}}$$

where ϵ_{opt} is the optimal convergence error of the diffusion model on the training distribution.

Therefore, the error term ζ satisfies:

$$|\zeta| \leq \mathcal{R}(\mathcal{P}, \tilde{\mathcal{P}}) \cdot \mathbf{W}(G_\theta^*, \mathcal{P}) \leq \mathcal{R}(\mathcal{P}, \tilde{\mathcal{P}}) \cdot \epsilon_{\text{opt}}$$

When \mathcal{P} and $\tilde{\mathcal{P}}$ are supported on the same manifold, $\text{diam}(\mathcal{A}) = \text{diam}(\tilde{\mathcal{A}})$, the geometric factor simplifies to depend only on the diameter of a single manifold. When the distribution shift increases, $\mathbf{W}(\mathcal{P}, \tilde{\mathcal{P}})$ increases, but the logarithmic term ensures a gentle growth of the geometric factor, which is consistent with the convergence behavior of diffusion models on manifolds. ■

Theorem 1 indicates that the minimum estimation error E_{\min} is primarily determined by the Wasserstein distance $\mathbf{W}(\mathcal{P}, \tilde{\mathcal{P}})$ between the deployment distribution and the true underlying radio propagation law, and is scaled by the influence factor $\mathcal{R}(\mathcal{P}, \tilde{\mathcal{P}})$. This factor captures the geometric differences in the underlying manifold structure of the data, and its theoretical form originates from the convergence bounds of diffusion models on compact manifolds. Note that E_{\min} is a function of the random variable ζ that depends on the gap between the diffusion model with random noise as its input and the training distribution.

B. Sampling-Dependent Estimation Error

Theorem 1 can be used to measure the effectiveness of diffusion models for radio map estimation, as it characterizes a lower bound for the best optimality gap that can be achieved by a diffusion model in theory. The optimality gap can be positive, indicating a discrepancy between the estimated and ground-truth radio maps, due to potential mismatches between the deployment domain distribution and the true underlying radio propagation law. As discussed in Section I, the problem of radio map estimation is challenging due to ultra-low sampling rates, where the number of available measurements is far smaller than the target map resolution. Intuitively, the quality of radio maps constructed by diffusion models improves as the input sampling rate increases. However, a major limitation of Theorem 1 is that the derived estimation error does not explicitly consider the sampling rate.

Define the estimation error E as

$$E = \|\mathbf{X} - \widetilde{\mathbf{M}}\|^2, \quad (15)$$

where \mathbf{X} is the map (matrix) predicted by a diffusion model. Given a sampling mask Ψ , the amount of information about the complete matrix $\widetilde{\mathbf{M}}$ provided by the observation matrix \mathbf{M} can be quantified by conditional mutual information:

$$\mathcal{I}(\Psi) = I(\widetilde{\mathbf{M}}; \mathbf{M}|\Psi) = H(\widetilde{\mathbf{M}}) - H(\widetilde{\mathbf{M}}|\mathbf{M}, \Psi) \quad (16)$$

where $H(\cdot)$ denotes differential entropy. This metric reflects the reduction in uncertainty about the complete matrix $\widetilde{\mathbf{M}}$ given the observation \mathbf{M} and the sampling pattern Ψ .

The efficacy of the generative model G_θ depends on its ability to effectively project observational information into the latent space \mathcal{Z} . Define the latent space information efficiency as:

$$\eta_z = \frac{I(\widetilde{\mathbf{M}}; G_\theta(\mathbf{Z}; \mathbf{M} \odot \Psi))}{I(\widetilde{\mathbf{M}}; \mathbf{M}|\Psi)} \cdot \frac{\dim(\mathcal{Z})}{\dim(\mathcal{M})} \quad (17)$$

where $\dim(\mathcal{Z})$ and $\dim(\mathcal{M})$ denote the dimensions of the latent space and the matrix space, respectively. This efficiency factor comprehensively reflects the compression efficiency and information retention capability of the latent space.

Based on the information-theoretic framework, considering the influence of the observational information amount $\mathcal{I}(\Psi)$ and the latent space efficiency η_z on the recovery error, we derive a model for E in the following theorem.

Theorem 2. *Given the minimum estimation error E_{min} defined in Eq. (13), the sampling mask Ψ , and the latent space efficiency η_z , the estimation error E satisfies:*

$$\begin{aligned} E &= E_{min} + E_{info} + E_{model} \\ &= \mathcal{R}(\mathcal{P}, \widetilde{\mathcal{P}}) \cdot \mathbf{W}(\mathcal{P}, \widetilde{\mathcal{P}}) \\ &\quad + \gamma \cdot \exp\left(-\lambda \cdot \frac{\mathcal{I}(\Psi)}{H(\widetilde{\mathbf{M}})} \cdot \eta_z^{\frac{\dim(\mathcal{M})}{\dim(\mathcal{Z})}}\right) + \epsilon \end{aligned} \quad (18)$$

where $\gamma > 0$ is the error sensitivity parameter, reflecting the amplification effect of missing observational information on the error; $\lambda > 0$ is the information decay coefficient, characterizing the marginal diminishing effect of information utilization, and $\epsilon \sim \mathcal{N}(0, \sigma^2)$ is the random disturbance term, encompassing uncertainties in model training and optimization.

Proof: The theoretical estimation error E can be decomposed into three interrelated components:

$$E = E_{min} + E_{info} + E_{model}$$

where E_{min} is defined by Eq. (13) in Theorem 1, E_{info} characterizes the error introduced by insufficient observational information, and E_{model} reflects the approximation error caused by imperfect latent space projection.

According to rate-distortion theory [43], under the condition of a given observational information amount $\mathcal{I}(\Psi)$, the minimum MSE achievable by the optimal estimation of the complete matrix $\widetilde{\mathbf{M}}$ satisfies:

$$\mathbb{E}[\|\mathbf{X} - \widetilde{\mathbf{M}}\|^2] \geq \sigma_{\widetilde{\mathbf{M}}}^2 \cdot \exp\left(-2 \cdot \frac{\mathcal{I}(\Psi)}{H(\widetilde{\mathbf{M}})}\right)$$

where \mathbf{X} is the estimation result, and $\sigma_{\widetilde{\mathbf{M}}}^2$ is the variance of $\widetilde{\mathbf{M}}$. However, due to the latent space bottleneck, the effective rate is reduced. Define the latent space information efficiency:

$$\eta_z = \frac{I(\widetilde{\mathbf{M}}; G_\theta(\mathbf{Z}; \mathbf{M} \odot \Psi))}{I(\widetilde{\mathbf{M}}; \mathbf{M}|\Psi)} \cdot \frac{\dim(\mathcal{Z})}{\dim(\mathcal{M})}$$

From the data processing inequality, $0 \leq \eta_z \leq 1$. The achievable effective rate becomes $R_{\text{eff}} = \eta_z^{\frac{d}{d_z}} \cdot \mathcal{I}(\Psi)$, where $d_z = \dim(\mathcal{Z})$, with the exponent arising from the concentration of measure phenomenon in information projection. Applying the rate-distortion bound with effective rate yields:

$$E_{info} = \gamma \cdot \exp\left(-\lambda \cdot \frac{\mathcal{I}(\Psi)}{H(\widetilde{\mathbf{M}})} \cdot \eta_z^{\frac{\dim(\mathcal{M})}{\dim(\mathcal{Z})}}\right)$$

where normalizing by $H(\widetilde{\mathbf{M}})$ makes the argument dimensionless, and $\gamma, \lambda > 0$ are constants depending on the model architecture.

Third, the model approximation error E_{model} arises from score estimation error and discretization. Under the assumptions of Section VI, the score estimation error satisfies:

$$\mathbb{E}_t \mathbb{E}_{\mathbf{x}(t)} [\|\mathbf{s}_\theta(\mathbf{x}(t), t) - \nabla \log p_t(\mathbf{x}(t))\|^2] \leq \epsilon_{\text{score}}^2$$

This error propagates to sample quality as $E_{model} \leq C_{\text{model}} \cdot \epsilon_{\text{score}}^{2\alpha}$. In practice, we absorb this into η_z , with remaining stochasticity captured by $\epsilon \sim \mathcal{N}(0, \sigma^2)$.

Finally, by the bias-variance decomposition, the total MSE combines these components additively when errors are uncorrelated, which holds asymptotically for well-behaved estimators. Therefore, we obtain:

$$E = E_{min} + \gamma \cdot \exp\left(-\lambda \cdot \frac{\mathcal{I}(\Psi)}{H(\widetilde{\mathbf{M}})} \cdot \eta_z^{\frac{\dim(\mathcal{M})}{\dim(\mathcal{Z})}}\right) + \epsilon$$

The exponential form for E_{info} is justified by the rate-distortion function's exponential decay, while the power exponent $\frac{\dim(\mathcal{M})}{\dim(\mathcal{Z})}$ captures the geometric effect of dimensionality reduction on information preservation.

From the perspective of Wasserstein geometry, the Wasserstein distance between the output distribution of the generative model G_θ under the observational condition $\mathbf{M} \odot \Psi$ and the target distribution $\widetilde{\mathcal{P}}$ satisfies:

$$\mathbf{W}(G_\theta(\cdot; \mathbf{M} \odot \Psi), \widetilde{\mathcal{P}}) \leq \mathbf{W}(\mathcal{P}, \widetilde{\mathcal{P}}) + \mathbf{W}(G_\theta(\cdot; \mathbf{M} \odot \Psi), \mathcal{P})$$

The first term on the right-hand side corresponds to E_{min} , and the second term is jointly influenced by the observational information amount and model efficiency, exhibiting a consistent trend of variation with $E_{info} + E_{model}$. ■

The proof of Theorem 1 is based on information projection theory and Wasserstein geometric properties. Theorem 1 not only quantifies the optimality gap of diffusion-based radio map estimation but also provides theoretical guidance for the joint optimization of model design and sampling strategies.

C. Sampling-Dependent Convergence Threshold

The estimation error E defined in Eq. (18) can be decomposed into three components:

$$E = E_{min} + E_{info} + E_{model} \quad (19)$$

where E_{min} is the minimum error defined in Eq. (13), $E_{info} = f(\mathcal{I}(\Psi))$ is the information deficiency error, arising from information loss due to sparse sampling, and $E_{model} = g(\eta_z)$ is the model approximation error, reflecting the imperfection of the latent space projection.

Considering that the functions $f(\cdot)$ and $g(\cdot)$ have the following asymptotic properties:

$$\lim_{\mathcal{I}(\Psi) \rightarrow H(\widetilde{\mathbf{M}})} f(\mathcal{I}(\Psi)) = 0, \quad \lim_{\eta_z \rightarrow 1} g(\eta_z) = 0 \quad (20)$$

and based on the error model in Theorem 2, we can derive conditions on radio sampling for diffusion models to achieve a given accuracy of radio map estimation.

Given an estimation error tolerance $\delta > 0$, under random sampling conditions, let ρ_c be a sampling rate (density) such that when sampling rates $\rho > \rho_c$, the estimation error E satisfies the following with a probability of at least $1 - \xi$:

$$\frac{E - E_{min}}{E_{min}} \leq \delta \quad (21)$$

Then we have the following theorem for ρ_c .

Theorem 3. *The sampling rate ρ_c satisfies:*

$$\rho_c = \min \left\{ \rho \in [0, 1] : \gamma \cdot \exp \left(-\lambda \cdot \frac{\mathcal{I}(\Psi_\rho)}{H(\widetilde{\mathbf{M}})} \cdot \eta_z^{\frac{\dim(\mathcal{M})}{\dim(\mathcal{Z})}} \right) \leq \delta \cdot E_{min} - \Phi^{-1}(1 - \xi) \cdot \sigma_\varepsilon \right\} \quad (22)$$

where Ψ_ρ denotes the sampling mask corresponding to ρ , and Φ^{-1} is the inverse cumulative distribution function of the standard normal distribution.

Proof: Recall that Theorem 2 provides the following decomposition of the estimation error for a given sampling mask Ψ :

$$E = E_{min} + \gamma \cdot \exp \left(-\lambda \cdot \frac{\mathcal{I}(\Psi)}{H(\widetilde{\mathbf{M}})} \cdot \eta_z^{\frac{\dim(\mathcal{M})}{\dim(\mathcal{Z})}} \right) + \varepsilon,$$

where $\varepsilon \sim \mathcal{N}(0, \sigma_\varepsilon^2)$ is a Gaussian disturbance independent of Ψ , and all other quantities are as defined in the main text. For a fixed sampling rate ρ , we consider a random sampling mask Ψ_ρ drawn from the distribution corresponding to ρ . In the regime of interest, the mutual information $\mathcal{I}(\Psi_\rho)$ depends on ρ in a deterministic manner (e.g., through its expectation under the random sampling scheme). Hence, we denote

$$A(\rho) \triangleq \frac{\mathcal{I}(\Psi_\rho)}{H(\widetilde{\mathbf{M}})} \cdot \eta_z^{\frac{\dim(\mathcal{M})}{\dim(\mathcal{Z})}},$$

which is a non-decreasing function of ρ because a higher sampling rate provides more information about the true radio map. The error term due to information deficiency then becomes $\Delta(\rho) = \gamma \exp(-\lambda A(\rho))$, which is non-increasing in ρ .

We aim to guarantee that, with probability at least $1 - \xi$, the relative error satisfies

$$\frac{E - E_{min}}{E_{min}} \leq \delta. \quad (23)$$

Substituting the expression for E , condition Eq. (23) is equivalent to

$$\Delta(\rho) + \varepsilon \leq \delta E_{min}. \quad (24)$$

Since ε is Gaussian and independent of Ψ_ρ , for a fixed ρ the probability of Eq. (24) is

$$\mathbb{P}(\Delta(\rho) + \varepsilon \leq \delta E_{min}) = \Phi \left(\frac{\delta E_{min} - \Delta(\rho)}{\sigma_\varepsilon} \right), \quad (25)$$

where Φ denotes the cumulative distribution function of the standard normal distribution. To ensure that this probability is at least $1 - \xi$, we require

$$\Phi \left(\frac{\delta E_{min} - \Delta(\rho)}{\sigma_\varepsilon} \right) \geq 1 - \xi. \quad (26)$$

Because Φ is strictly increasing, Eq. (26) is equivalent to

$$\frac{\delta E_{min} - \Delta(\rho)}{\sigma_\varepsilon} \geq \Phi^{-1}(1 - \xi), \quad (27)$$

where Φ^{-1} is the quantile function of the standard normal distribution. Rearranging gives

$$\Delta(\rho) \leq \delta E_{min} - \sigma_\varepsilon \Phi^{-1}(1 - \xi). \quad (28)$$

Recalling the definition of $\Delta(\rho)$, inequality Eq. (28) becomes

$$\gamma \exp(-\lambda A(\rho)) \leq \delta E_{min} - \sigma_\varepsilon \Phi^{-1}(1 - \xi). \quad (29)$$

The right-hand side of Eq. (29) is assumed to be positive for the threshold to be meaningful; otherwise any ρ would satisfy the condition. Because $A(\rho)$ increases with ρ , the left-hand side decreases with ρ . Therefore, the set of ρ for which Eq. (29) holds is an interval $[\rho_c, 1]$, where ρ_c is the smallest ρ satisfying Eq. (29). Formally,

$$\rho_c = \min \{ \rho \in [0, 1] : \gamma \cdot \exp(-\lambda \cdot A(\rho)) \leq \delta \cdot E_{min} - \Phi^{-1}(1 - \xi) \cdot \sigma_\varepsilon \}$$

Substituting back the definition of $A(\rho)$ yields exactly the expression in Theorem 3. \blacksquare

Theorem 3 extends Eq. (1) to the setting of diffusion-based radio map estimation, and offers theoretical guidance for sampling strategy design: When the sampling rate falls below ρ_c , the quality of the estimated radio maps improves substantially with increasing sampling rates; once the sampling rate exceeds ρ_c , further increases yield only marginal gains.

VIII. APPROXIMATIONS TO THEORETICAL RADIO MAP ESTIMATION ERRORS OF DIFFUSION MODELS

In the previous section, for the problem of radio map estimation, we derived a theoretical minimum estimation error that can be achieved by diffusion models (Theorem 1), and further extended this error to incorporate the sampling rate (Theorem 2). However, direct application of these error bounds in practical scenarios is hindered by their reliance on information that is often unavailable or difficult to obtain. To address this limitation, in this section, we introduce empirical formulas which approximate the derived errors and are readily computable in practice.

A. Approximation to Minimum Estimation Error

For the minimum estimation error E_{\min} in Eq. (13), $\text{diam}(\mathcal{A})$ (diameter of the manifold \mathcal{A}), $\text{diam}(\tilde{\mathcal{A}})$ (diameter of the manifold $\tilde{\mathcal{A}}$), and $\mathbf{W}(\mathcal{P}, \tilde{\mathcal{P}})$ (Wasserstein distance between distributions \mathcal{P} and $\tilde{\mathcal{P}}$) are difficult to calculate in practice. However, since datasets are empirical samples drawn from the underlying radio map distributions, they can serve as practical proxies for this distributional information. Leveraging principles from probability theory and statistics, we therefore approximate $\text{diam}(\mathcal{A})$, $\text{diam}(\tilde{\mathcal{A}})$, and $\mathbf{W}(\mathcal{P}, \tilde{\mathcal{P}})$ using observable datasets and their empirical similarity. The proposed approximations are formalized in the following corollary.

Corollary 1. *The following E_{\min}^* approximates the minimum estimation error E_{\min} in Eq. (13):*

$$E_{\min}^* = C' \cdot \left(\frac{\text{diam}(Y) + \text{diam}(\tilde{Y})}{2} \right) \cdot \left(1 + \log \left(1 + D(Y, \tilde{Y}) \right) \right) \cdot D(Y, \tilde{Y}) + \tilde{\zeta} \quad (30)$$

where $D(Y, \tilde{Y})$ is a distribution difference metric computed based on the datasets Y and \tilde{Y} , used to approximate the theoretical Wasserstein distance and can be measured by methods such as Fréchet Inception Distance (FID) [44] and Maximum Mean Discrepancy (MMD) [45]. Here, Y and \tilde{Y} are finite datasets from the target distribution and the training distribution, respectively; $\text{diam}(\cdot)$ denotes the empirical diameter of a dataset (e.g., the maximum distance between samples); C' is a fitting constant related to the model and task. $\tilde{\zeta}$ is an error term reflecting the empirical approximation error of the diffusion model G_θ on its training distribution \tilde{Y} , which can be estimated through the model's performance on a held-out test set from the training distribution.

The empirical formula in Eq. (30) provides a practical approximation of the minimum estimation error in Eq. (13). Specifically, it uses the maximum distance between samples in the dataset Y to approximate the diameter of the manifold \mathcal{A} , uses the maximum distance between samples in the dataset \tilde{Y} to approximate the diameter of the manifold $\tilde{\mathcal{A}}$, and uses FID or MMD to approximate the Wasserstein distance between \mathcal{P} and $\tilde{\mathcal{P}}$. Unlike its theoretical counterpart, Eq. (30) is readily computable in practice and thus well-suited for real-world applications. Corollary 1 suggests that our proposed approximation to the minimum estimation error is related to the distributional difference between the dataset used for model training and the dataset used for model inference. Similar to E_{\min} defined in Eq. (13), E_{\min}^* is a function of the random variable $\tilde{\zeta}$ that depends on the gap between the diffusion model with random noise as its input and the training dataset.

B. Approximation to Sampling-Dependent Estimation Error

For the estimation error E defined in Eq. (18), information-related metrics, e.g., the mutual information $\mathcal{I}(\Psi)$ and the differential entropy $H(\tilde{\mathbf{M}})$, are difficult to calculate in practice. In the following corollary, we provide an empirical formula to approximate E .

Corollary 2. *Considering that the layout of obstacles and the degree of radio power variation near sampling points significantly impact the estimation of radio maps, we propose to use the following E^* to approximate the sampling-dependent estimation error E in Eq. (18):*

$$E^* = E_{\min}^* + E_{\text{model}}^* - \alpha \ln(\rho^* + 1) + \epsilon \quad (31)$$

with

$$\rho^* = \frac{c_1 \cdot (\kappa + c_2) \cdot (\rho + c_3)}{\exp \left[\frac{1}{mn} \sum_{i=1}^m \sum_{j=1}^n \mathbf{B}_{ij} \right]} \quad (32)$$

where ρ represents the actual sampling rate, \mathbf{B} is the obstacle layout mask, with 1 indicating the locations of the obstacles and 0 for others, c_1, c_2, c_3 are normalization hyperparameters, and κ represents the degree of power variation at sampling points and can be computed as:

$$\kappa = \frac{\Psi \odot \sqrt{(\nabla_x \mathbf{X})^2 + (\nabla_y \mathbf{X})^2}}{\sum_{i=1}^m \sum_{j=1}^n \Psi_{ij}} \quad (33)$$

Let \mathbf{X}_{true} be the true matrix of a radio map, and Ψ_{train} and Ψ_{test} be the training and test sampling masks, respectively. Then we have

$$E_{\text{model}}^* = \mathbf{W}(G_{\theta^*}(\cdot; \Psi_{\text{train}}), \mathcal{P}_{\text{train}}) + \mathbf{W}(\mathcal{P}_{\text{train}}, \mathcal{P}_{\text{test}}) + \mathbf{W}(G_{\theta^*}(\cdot; \Psi_{\text{test}}), G_{\theta^*}(\cdot; \Psi_{\text{train}})) \quad (34)$$

where $\mathcal{P}_{\text{train}} = \mathcal{P}(\cdot | \mathbf{X}_{\text{true}} \odot \Psi_{\text{train}})$ and $\mathcal{P}_{\text{test}} = \mathcal{P}(\cdot | \mathbf{X}_{\text{true}} \odot \Psi_{\text{test}})$. For brevity, denote $G_\theta(\cdot; \Psi) \equiv G_\theta(\mathbf{Z}; \mathbf{X}_{\text{true}} \odot \Psi)$. In addition, let θ^* denote the model parameters optimized on the training dataset, aiming to minimize the training distribution matching error and the observation reconstruction error:

$$\theta^* = \arg \min_{\theta} \mathbf{W}(G_\theta(\cdot; \Psi_{\text{train}}), \mathcal{P}_{\text{train}}) + \lambda \| (G_\theta(\cdot; \Psi_{\text{train}}) - \mathbf{X}_{\text{true}}) \odot \Psi_{\text{train}} \|_F^2. \quad (35)$$

The empirical formula in Eq. (31) provides a practical approximation of the sampling-dependent estimation error in Eq. (18). Specifically, as shown in Eq. (19), the sampling-dependent estimation error consists of the minimum estimation error (defined in Eq. (13)), the information deficiency error (arising from information loss due to sparse sampling), and the model approximation error (reflecting the imperfection of the latent space projection). Eq. (31) uses Eq. (30) in Corollary 1 to approximate the minimum estimation error, leverages the layout of obstacles and the degree of radio power variation near sampling points, both of which significantly impact the estimation of radio maps, to approximate the information deficiency error, and employs the differences between training dataset and test dataset to approximate the model approximation error.

C. Training Sampling Rate vs Test Sampling Rate

As shown in Eq. (18) and Eq. (31), the estimation error comprises a model approximation component that depends primarily on model characteristics and the distributional discrepancy between the training and test datasets. In the context of diffusion-based radio map estimation, the sampling rate employed during training may differ from that used during

testing. Intuitively, the training sampling rate should be no smaller than the test sampling rate, as the model is optimized on the training sampling rate and may not generalize well to higher-rate inputs unseen during training. However, *to improve the test-time performance of a diffusion model for radio map estimation, should the test-time sampling rate be equal to, or less than the training-time sampling rate?* In this section, we address this question by analyzing the model approximation error derived in Eq. (34).

Let the sampling rate during training be ρ_{train} and that during test be ρ_{test} with $\rho_{\text{train}} \geq \rho_{\text{test}}$, then we have the following corollary.

Corollary 3. *Given a test sampling rate ρ_{test} , there exists a training sampling rate $\rho_{\text{train}}^* > \rho_{\text{test}}$ that minimizes Eq. (34) which approximates the model approximation error.*

Based on Eq. (34), consider

$$\begin{aligned}
 E_{\text{model}}^* &= \underbrace{\mathbf{W}(G_{\theta^*}(\cdot; \Psi_{\text{train}}), \mathcal{P}_{\text{train}})}_{(A)} \\
 &+ \underbrace{\mathbf{W}(\mathcal{P}_{\text{train}}, \mathcal{P}_{\text{test}})}_{(B)}, \\
 &+ \underbrace{\mathbf{W}(G_{\theta^*}(\cdot; \Psi_{\text{test}}), G_{\theta^*}(\cdot; \Psi_{\text{train}}))}_{(C)}
 \end{aligned} \tag{36}$$

In the following, we analyze each term and derive Corollary 3.

Training Distribution Matching Error (A) This term characterizes the model’s fit to the training conditional distribution. Since $\rho_{\text{train}} \geq \rho_{\text{test}}$, the training phase provides more observational information, enabling the model to better learn the underlying radio propagation laws. Therefore, assuming sufficient model capacity, (A) monotonically decreases as ρ_{train} increases. Denote (A) as $f(\rho_{\text{train}})$, where $f(\cdot)$ is a decreasing function.

Conditional Distribution Shift Term (B) This term reflects the difference in true distributions caused by differing observation conditions. Based on the physical smoothness and local correlation of radio propagation, there exists a constant $L > 0$ such that the Wasserstein distance between two conditional distributions satisfies:

$$\mathbf{W}(\mathcal{P}(\cdot|\Psi_1), \mathcal{P}(\cdot|\Psi_2)) \leq L \cdot \mathbb{E}_{(i,j)}[|\Psi_1(i,j) - \Psi_2(i,j)|]. \tag{37}$$

When Ψ_{train} and Ψ_{test} are sampled i.i.d., the expected difference is $|\rho_{\text{train}} - \rho_{\text{test}}|$, thus (B) $\leq L \cdot |\rho_{\text{train}} - \rho_{\text{test}}|$.

Conditional Input Difference Term (C) This term measures the sensitivity of the model output to changes in the input mask. For a sufficiently trained diffusion model that robustly understands radio propagation laws, its output distribution should remain stable to small perturbations in the input. Assuming that the model satisfies Lipschitz continuity, there exists a constant $K > 0$ such that:

$$\mathbf{W}(G_{\theta^*}(\cdot; \Psi_1), G_{\theta^*}(\cdot; \Psi_2)) \leq K \cdot \mathbb{E}_{(i,j)}[|\Psi_1(i,j) - \Psi_2(i,j)|], \tag{38}$$

thus (C) $\leq K \cdot |\rho_{\text{train}} - \rho_{\text{test}}|$.

Combining the above analysis, the model approximation error is upper bounded by:

$$\mathbb{E}[\mathcal{E}_{\text{approx}}] \leq f(\rho_{\text{train}}) + (L + K) \cdot (\rho_{\text{train}} - \rho_{\text{test}}). \tag{39}$$

When the test sampling rate ρ_{test} is fixed, the upper bound $f(\rho_{\text{train}}) + (L + K) \cdot (\rho_{\text{train}} - \rho_{\text{test}})$ first decreases and then increases with ρ_{train} ($\rho_{\text{train}} \geq \rho_{\text{test}}$): initially, when ρ_{train} increases, the rapid decrease of $f(\rho_{\text{train}})$ dominates, causing the upper bound to decrease; as ρ_{train} increases further, the growth of the linear term $(L + K)(\rho_{\text{train}} - \rho_{\text{test}})$ gradually dominates, leading to an increase in the upper bound. Therefore, there exists an optimal $\rho_{\text{train}}^* > \rho_{\text{test}}$ that minimizes the upper bound of $\mathbb{E}[\mathcal{E}_{\text{approx}}]$.

Corollary 3 establishes that, for diffusion-based radio map estimation, setting the training sampling rate slightly above the test sampling rate achieves an optimal trade-off. This configuration balances two competing effects: it provides sufficient training data for the model to learn the underlying radio propagation laws and effectively complete missing information, while avoiding excessive conditional mismatch that would degrade performance in low-sampling test scenarios. Specifically, when $\rho_{\text{train}} = \rho_{\text{test}}$, the model may lack the capacity to generalize beyond the observed samples; when $\rho_{\text{train}} \gg \rho_{\text{test}}$, the disparity in sampling conditions impairs the model’s ability to perform accurately under the test-time sampling regime.

IX. NUMERICAL RESULTS

In this section, we use large-scale simulations to evaluate our proposed empirical formulas which approximate our derived theoretical performance bounds by diffusion models for radio map estimation.

A. Simulation Setup

We use the open-source radio map dataset *BART-Lab radio maps*¹ from [46] for evaluation. This dataset is obtained by the simulation software *Altair Feko* from *WinProp* [47] and consists of 2000 radio maps. The number of transmitters in one radio map varies from 1 to 3. There are 2000 different layouts of buildings in the dataset, extracted from *OpenStreetMap* [48] in the United States. The heights of the buildings are set as 10 m. This dataset consists of radio maps simulated in 5 different frequency bands: 1750 MHz, 2750 MHz, 3750 MHz, 4750 MHz, and 5750 MHz. We select the 5750 MHz subset for evaluation. Considering that the resolutions of the original maps in the dataset are different, to ensure consistency, we randomly extract 256×256 (i.e., $m = n = 256$) regions from each map. This results in 1776 different radio maps, each of which has a resolution of 256×256 . Among them, 1676 are used for model training and the remaining 100 are used for test. During test, the sampling rate varies from $1/(256 \times 256) = 0.002\%$ to $300/(256 \times 256) = 0.458\%$. For a given sampling rate, radio samples are randomly distributed within the region of interest.

¹<https://github.com/BRATLab-UCD/Radiomap-Data>

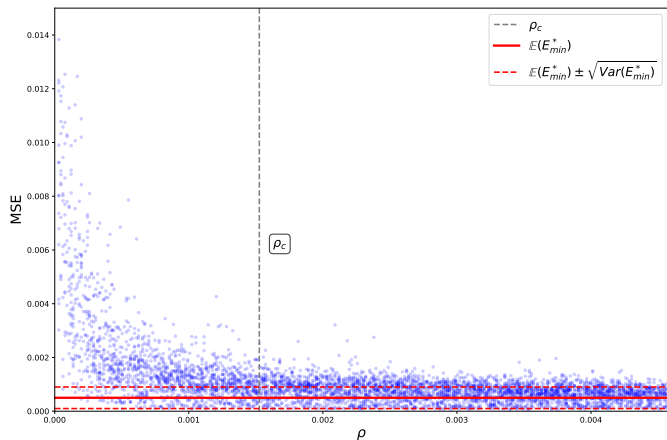


Fig. 4: Simulation results to evaluate Corollary 1.

We simulate *WiFi-Diffusion* from [9] to evaluate our proposed empirical formulas. *WiFi-Diffusion* first uses DDPM, a well-known diffusion model, to generate a candidate set of radio maps (64 radio maps in simulations) with diverse qualities under ultra-low sampling rates, and then employs principles of radio propagation to identify the most accurate map. We implement *WiFi-Diffusion* on an NVIDIA RTX 4090 GPU and an AMD EPYC 9654 CPU. Deep learning codes are built using PyTorch.

B. Simulation Results

Evaluation on Corollary 1 In Theorem 1, we derived E_{\min} , the minimum error that can be achieved by a diffusion model for radio map estimation. Since direct computation of E_{\min} is difficult in practice, in Corollary 1, we introduced an empirical approximation E_{\min}^* that is readily computable. To assess the fidelity of this approximation, we conduct 5000 simulation instances, each with a sampling rate ρ randomly drawn from the interval $[0.002\%, 0.458\%]$. Fig. 4 illustrates the resulting MSE for each instance.

Fig. 4 reveals variability in the quality of maps produced by *WiFi-Diffusion*, attributable to the stochastic nature of diffusion models (the dependence of the diffusion model’s output on a random input noise). Moreover, in the figure, the solid red line represents the expectation of E_{\min}^* (recall that as discussed in Section VIII-A, E_{\min}^* is a function of the random variable $\tilde{\zeta}$), while the dashed red lines indicate the standard deviation of E_{\min}^* . Comparing these red lines with the MSE values of individual instances, we observe that E_{\min}^* is an effective approximation to the minimum estimation error, as the majority of MSE values lie close to the expectation and within one standard deviation, with only minor deviations.

In Theorem 3, we derived a sampling rate threshold ρ_c for diffusion models to achieve convergence. In Fig. 4, we also present ρ_c . From the figure, we observe that as the sampling rate exceeds ρ_c , the quality of radio maps constructed by *WiFi-Diffusion* remains relatively stable as the sampling rate increases, which again verifies the effectiveness of our empirical formula E_{\min}^* .

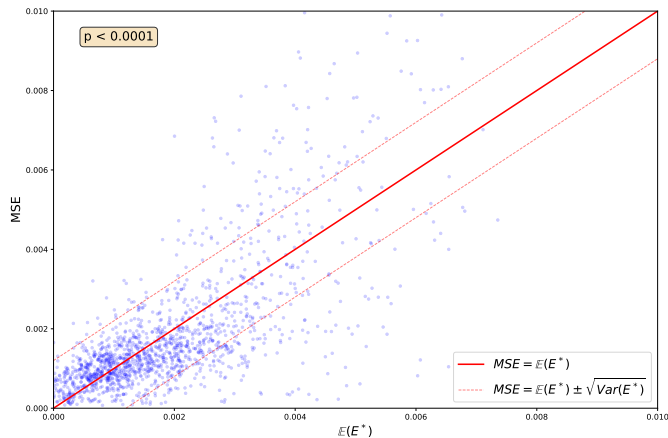


Fig. 5: Simulation results to evaluate Corollary 2.

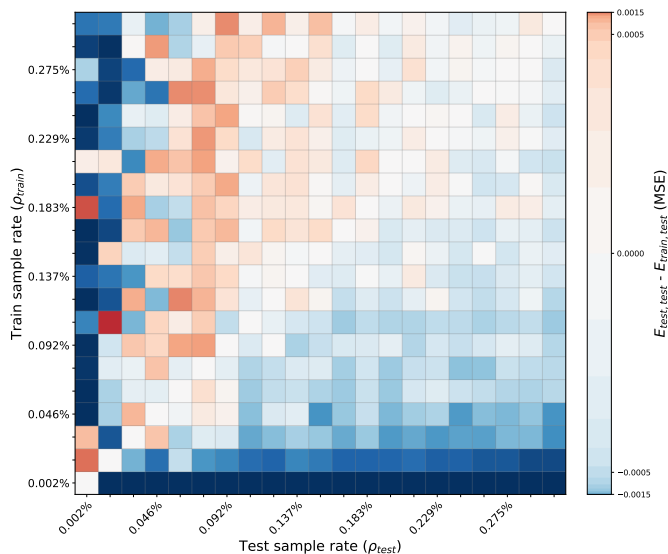


Fig. 6: Simulation results to evaluate Corollary 3.

Evaluation on Corollary 2 In Theorem 2, we derived E , the sampling-dependent estimation error that can be achieved by a diffusion model for radio map estimation. Since direct computation of E is difficult in practice, in Corollary 2, we introduced an empirical approximation E^* that is readily computable. To validate the effectiveness of this approximation, we conducted simulations and present the results in Fig. 5. Specifically, for each simulated instance with a sampling rate below 0.0001, we plot the MSE of the reconstructed radio map (y-axis) against the corresponding expectation of E^* (x-axis). We focus on low sampling rates because the estimation error E is most sensitive to sampling density in this regime, i.e., the deviation between E and the minimum error E_{\min} becomes pronounced. The figure confirms that E^* serves as a reliable approximation of E : most data points are near the diagonal line, indicating close agreement between the achieved MSE and the derived error bound.

Evaluation on Corollary 3 In Corollary 3, we established that for diffusion models, given a fixed test-time sampling rate, setting the training sampling rate slightly above the test

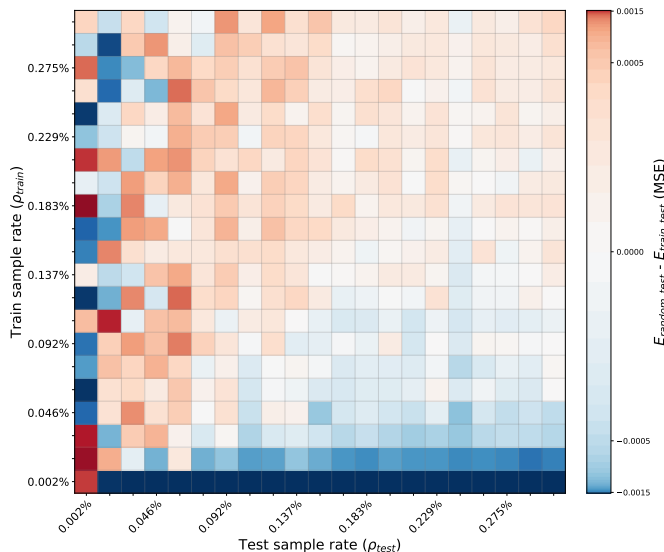


Fig. 7: Simulation results comparing diffusion models trained with random sampling rates with those trained with a fixed sampling rate.

sampling rate minimizes the estimation error at test time. We now present simulation results to validate this corollary. Consider the following set of sampling rates P :

$$P = \{0.002\%, 0.015\%, 0.031\%, 0.046\%, 0.061\%, 0.076\%, 0.092\%, 0.107\%, 0.122\%, 0.137\%, 0.153\%, 0.168\%, 0.183\%, 0.198\%, 0.214\%, 0.229\%, 0.244\%, 0.259\%, 0.275\%, 0.290\%, 0.305\%\}.$$

For each $\rho_{\text{train}} \in P$, we trained a diffusion model using that sampling rate. Then each trained model was evaluated on every $\rho_{\text{test}} \in P$, yielding a total of 21×21 MSE values corresponding to all pairs $(\rho_{\text{test}}, \rho_{\text{train}})$. The results are visualized in Fig. 6.

In Fig. 6, each cell indexed by $(\rho_{\text{test}}, \rho_{\text{train}})$ displays the MSE difference $E_{\text{test,test}} - E_{\text{train,test}}$, where $E_{\text{test,test}}$ denotes the MSE of a model trained and tested at the same sampling rate ρ_{test} , while $E_{\text{train,test}}$ denotes the MSE of a model trained at ρ_{train} and tested at ρ_{test} . A larger value of this difference (indicated by a redder cell in the figure) suggests that the model trained at ρ_{train} outperforms the baseline model trained and tested at ρ_{test} . From Fig. 6, we observe that for each $\rho_{\text{test}} \in P$, the maximum difference occurs in the region above the diagonal, i.e., where $\rho_{\text{train}} > \rho_{\text{test}}$. This confirms that the optimal training sampling rate for a given test rate exceeds the test rate itself, thereby validating Corollary 3.

More Simulation Results We note that diffusion models can also be trained using random sampling rates, where each training instance employs a potentially different sampling rate. This raises an interesting question: Does training with random sampling rates yield better performance than training with a fixed sampling rate? Finally, we conducted simulations to address this question.

In Fig. 7, each cell indexed by $(\rho_{\text{test}}, \rho_{\text{train}})$ displays the MSE difference $E_{\text{random,test}} - E_{\text{train,test}}$, where $E_{\text{random,test}}$ denotes the MSE of a model trained at random sampling rates (i.e., for

each training instance, the sampling rate is drawn uniformly from P) and tested at ρ_{test} , while $E_{\text{train,test}}$ denotes the MSE of a model trained at a fixed rate ρ_{train} and tested at ρ_{test} . A positive value of this difference (indicated by a warmer color in the figure) indicates that the fixed-rate model outperforms the random-rate model. From the figure, we observe that for each $\rho_{\text{test}} \in P$, the maximum difference occurs in the region above the diagonal. This result demonstrates that training with a fixed sampling rate, particularly one slightly above the test rate, yields superior radio map estimation performance compared to training with random sampling rates.

X. CONCLUSION

The radio map estimation problem requires one to construct a radio map from limited radio samples collected by sensors sparsely distributed within a region of interest. It is challenging to solve the problem due to the extreme sparsity of radio samples relative to map resolution. While diffusion models have recently emerged as a promising approach for this problem, their theoretical performance has remained unexplored. This work provides the missing theoretical foundation.

Specifically, by formulating radio map estimation as a non-linear matrix completion problem, we first derive a theoretical lower bound on the minimum estimation error that can be achieved by diffusion models. We then extend this bound to take sampling rate into consideration, capturing the additional error introduced by ultra-sparse sampling. Furthermore, we establish a critical sampling rate threshold necessary for diffusion models to achieve performance convergence. Finally, as we note that the derived error bounds rely on certain information difficult to obtain in practice, we propose empirical formulas which approximate error bounds and are readily computable from observable data. Extensive simulations verify that our proposed approximations are tight.

As future research directions, we plan to design diffusion-based radio map estimation models that surpass current approaches and approach the theoretical accuracy bounds established in this work, and develop radio sampling strategies adaptive to dynamic environments, enhancing the estimation performance of diffusion models.

REFERENCES

- [1] D. Romero and S.-J. Kim, "Radio map estimation: A data-driven approach to spectrum cartography," *IEEE Signal Processing Magazine*, vol. 39, no. 6, pp. 53–72, 2022.
- [2] Y. Peng, Y. Li, Y. Guo, D. Zhang, F. Khan, R. Alturki, and B. Alshawi, "A blockchain-based distributed collaborative sensing and spectrum access approach for consumer electronics," *IEEE Transactions on Consumer Electronics*, 2025, early access.
- [3] A. S. Matar and X. Shen, "Joint optimization of user association, power control, and dynamic spectrum sharing for integrated aerial-terrestrial network," *IEEE Journal on Selected Areas in Communications*, vol. 43, no. 1, pp. 396–409, 2025.
- [4] J. ZHAO *et al.*, "CSELM-QE: A composite semi-supervised extreme learning machine with unlabeled rssi quality estimation for radio map construction," *Chinese Journal of Electronics*, vol. 29, no. 6, pp. 1016–1024, 2020.
- [5] J. Huang, L. Lian, D. Wen, Y. Zhou, F. Wang, W. Wang, and Y. Shi, "Dynamic UAV-assisted cooperative edge AI inference," *IEEE Transactions on Wireless Communications*, vol. 24, no. 1, pp. 615–628, 2024.
- [6] R. Levie, Ç. Yapar, G. Kutyniok, and G. Caire, "RadioUNet: Fast radio map estimation with convolutional neural networks," *IEEE Transactions on Wireless Communications*, vol. 20, no. 6, pp. 4001–4015, 2021.

- [7] W. Locke, N. Lohmachev, Y. Huang, and X. Li, "Radio map estimation with deep dual path autoencoders and skip connection learning," in *Proc. of IEEE PIMRC, Toronto, Canada, September 05-08, 2023*.
- [8] X. Li, S. Zhang, H. Li, X. Li, L. Xu, H. Xu, H. Mei, G. Zhu, N. Qi, and M. Xiao, "RadioGAT: A joint model-based and data-driven framework for multi-band radiomap reconstruction via graph attention networks," *IEEE Transactions on Wireless Communications*, vol. 23, no. 11, pp. 1–1, 2024.
- [9] Z. Liu, S. Zhang, Q. Liu, H. Zhang, and L. Song, "Wifi-diffusion: Achieving fine-grained wifi radio map estimation with ultra-low sampling rate by diffusion models," *IEEE Journal on Selected Areas in Communications*, vol. 43, no. 11, pp. 3796–3812, 2025.
- [10] K. Rizk, J.-F. Wagen, and F. Gardiol, "Two-dimensional ray-tracing modeling for propagation prediction in microcellular environments," *IEEE Transactions on Vehicular Technology*, vol. 46, no. 2, pp. 508–518, 1997.
- [11] R. Wahl, G. Wölffe, P. Wildbolz, and F. Landstorfer, "Dominant path prediction model for urban scenarios," in *Proc. of IST Mobile and Wireless Communications, Dresden, Germany, June 19-23, 2005*.
- [12] T. Zugno, M. Drago, M. Giordani, M. Polese, and M. Zorzi, "Toward standardization of millimeter-wave vehicle-to-vehicle networks: Open challenges and performance evaluation," *IEEE Communications Magazine*, vol. 58, no. 9, pp. 79–85, 2020.
- [13] C. M. Bishop, *Neural Networks for Pattern Recognition*. New York, NY, USA: Oxford University Press, Inc., 1995.
- [14] J. A. Bazerque, G. Mateos, and G. B. Giannakis, "Group-lasso on splines for spectrum cartography," *IEEE Transactions on Signal Processing*, vol. 59, no. 10, pp. 4648–4663, 2011.
- [15] G. Boccolini, G. Hernández-Peñaloza, and B. Beferull-Lozano, "Wireless sensor network for spectrum cartography based on kriging interpolation," in *Proc. of IEEE PIMRC, Sydney, Australia, September 09-12, 2012*.
- [16] X. Wang, K. Tao, N. Cheng, Z. Yin, Z. Li, Y. Zhang, and X. Shen, "Radiodiff: An effective generative diffusion model for sampling-free dynamic radio map construction," *IEEE Transactions on Cognitive Communications and Networking*, vol. 11, no. 2, pp. 738–750, 2025.
- [17] X. Luo, Z. Li, Z. Peng, M. Chen, and Y. Liu, "Denoising diffusion probabilistic model for radio map estimation in generative wireless networks," *IEEE Transactions on Cognitive Communications and Networking*, vol. 11, no. 2, pp. 751–763, 2025.
- [18] K. Qiu, S. Bakirtzis, I. Wassell, H. Song, K. Lin, and J. Zhang, "IRDM: A generative diffusion model for indoor radio map interpolation," in *Proc. of IEEE Global Communications Conference, Kuala Lumpur, Malaysia, December 4–8, 2023*.
- [19] D. Romero, T. N. Ha, R. Shrestha, and M. Franceschetti, "Theoretical analysis of the radio map estimation problem," *IEEE Transactions on Wireless Communications*, vol. 23, no. 10, pp. 13 722–13 737, 2024.
- [20] Y. Zhang and S. Wang, "K-nearest neighbors gaussian process regression for urban radio map reconstruction," *IEEE Communications Letters*, vol. 26, no. 12, pp. 3049–3053, 2022.
- [21] D. Denkovski, V. Atanasovski, L. Gavrilovska, J. Riihijärvi, and P. Mähönen, "Reliability of a radio environment map: Case of spatial interpolation techniques," in *2012 7th International ICST Conference on Cognitive Radio Oriented Wireless Networks and Communications (CROWNCOM)*, 2012, pp. 248–253.
- [22] S. Shao, L. Cheng, K. Chen, Q. Liu, S. Zhang, H. Zhang, and L. Song, "Collaboradio: A hybrid device-edge-cloud collaboration paradigm for fine-grained radio map construction," *IEEE Transactions on Mobile Computing*, vol. 25, no. 1, pp. 599–613, 2026.
- [23] S. Zhang, A. Wijesinghe, and Z. Ding, "Rme-gan: A learning framework for radio map estimation based on conditional generative adversarial network," *IEEE Internet of Things Journal*, vol. 10, no. 20, pp. 18 016–18 027, 2023.
- [24] H. Jia, N. Cheng, X. Wang, C. Zhou, R. Sun, and X. Shen, "RadioMamba: Breaking the accuracy-efficiency trade-off in radio map construction via a hybrid mamba-unet," *IEEE Transactions on Network Science and Engineering*, pp. 1–14, 2025.
- [25] Q. Gao, Q. Zhu, Z. Lin, P. T. Mathiopoulos, Y. Zhao, Y. Huang, J. Wang, and Q. Wu, "Time-variant radio map reconstruction with optimized distributed sensors in dynamic spectrum environments," *IEEE Internet of Things Journal*, vol. 12, no. 12, pp. 20 927–20 941, 2025.
- [26] X. Jang, T. Li, Z. Xiao, K. Chen, S. Ma, Z. Wang, and K. Li, "UniRM: A universal large model for multiband 3d radio map construction," *IEEE Journal on Selected Areas in Communications*, vol. 44, pp. 2244–2258, 2026.
- [27] E. J. Candès and B. Recht, "Exact matrix completion via convex optimization," *Foundations of Computational Mathematics*, vol. 9, no. 6, pp. 717–772, Dec. 2009. [Online]. Available: <https://doi.org/10.1007/s10208-009-9045-5>
- [28] X. Su and T. M. Khoshgoftaar, "A survey of collaborative filtering techniques," *Advances in Artificial Intelligence*, vol. 2009, no. 1, p. 421425, 2009. [Online]. Available: <https://onlinelibrary.wiley.com/doi/abs/10.1155/2009/421425>
- [29] K. H. Jin and J. C. Ye, "Annihilating filter-based low-rank hankel matrix approach for image inpainting," *IEEE Transactions on Image Processing*, vol. 24, no. 11, pp. 3498–3511, 2015.
- [30] J. Ma, Z. Tian, H. Zhang, and T. W. Chow, "Multi-label low-dimensional embedding with missing labels," *Knowledge-Based Systems*, vol. 137, pp. 65–82, 2017. [Online]. Available: <https://www.sciencedirect.com/science/article/pii/S0950705117304136>
- [31] L. T. Nguyen, J. Kim, and B. Shim, "Low-rank matrix completion: A contemporary survey," *IEEE Access*, vol. 7, pp. 94 215–94 237, 2019.
- [32] J. Fan and T. W. Chow, "Non-linear matrix completion," *Pattern Recognition*, vol. 77, pp. 378–394, 2018. [Online]. Available: <https://www.sciencedirect.com/science/article/pii/S0031320317304028>
- [33] J. Fan and J. Cheng, "Matrix completion by deep matrix factorization," *Neural Networks*, vol. 98, pp. 34–41, 2018. [Online]. Available: <https://www.sciencedirect.com/science/article/pii/S0893608017302502>
- [34] S. Si, K.-Y. Chiang, C.-J. Hsieh, N. Rao, and I. S. Dhillon, "Goal-directed inductive matrix completion," in *Proceedings of the 22nd ACM SIGKDD International Conference on Knowledge Discovery and Data Mining*, ser. KDD '16. New York, NY, USA: Association for Computing Machinery, 2016, p. 1165–1174. [Online]. Available: <https://doi.org/10.1145/2939672.2939809>
- [35] Y. Song, J. Sohl-Dickstein, D. P. Kingma, A. Kumar, S. Ermon, and B. Poole, "Score-based generative modeling through stochastic differential equations," in *International Conference on Learning Representations*, 2021. [Online]. Available: <https://openreview.net/forum?id=PxTIG12RRHS>
- [36] B. Øksendal, *Stochastic Differential Equations*. Berlin, Heidelberg: Springer Berlin Heidelberg, 2003, pp. 65–84. [Online]. Available: https://doi.org/10.1007/978-3-642-14394-6_5
- [37] B. D. Anderson, "Reverse-time diffusion equation models," *Stochastic Processes and their Applications*, vol. 12, no. 3, pp. 313–326, 1982. [Online]. Available: <https://www.sciencedirect.com/science/article/pii/0304414982900515>
- [38] Y. Song and S. Ermon, "Generative modeling by estimating gradients of the data distribution," in *Advances in Neural Information Processing Systems*, 2019, pp. 11 895–11 907.
- [39] —, "Generative modeling by estimating gradients of the data distribution," in *Advances in Neural Information Processing Systems*, 2019, pp. 11 895–11 907.
- [40] J. Ho, A. Jain, and P. Abbeel, "Denoising diffusion probabilistic models," in *Proc. of NeurIPS, virtual only conference, December 06-12, 2020*.
- [41] V. D. Bortoli, "Convergence of denoising diffusion models under the manifold hypothesis," *Transactions on Machine Learning Research*, 2022, expert Certification. [Online]. Available: <https://openreview.net/forum?id=MhK5aXo3gB>
- [42] B. Fesl, B. Böck, F. Strasser, M. Baur, M. Joham, and W. Utschick, "On the asymptotic mean square error optimality of diffusion models," in *Proceedings of The 28th International Conference on Artificial Intelligence and Statistics*, ser. Proceedings of Machine Learning Research, Y. Li, S. Mandt, S. Agrawal, and E. Khan, Eds., vol. 258. PMLR, 03–05 May 2025, pp. 505–513. [Online]. Available: <https://proceedings.mlr.press/v258/fesl25a.html>
- [43] J. D. Gibson, *Rate Distortion Theory*. Cham: Springer Nature Switzerland, 2025, pp. 77–92. [Online]. Available: https://doi.org/10.1007/978-3-031-65388-9_12
- [44] M. Heusel, H. Ramsauer, T. Unterthiner, B. Nessler, and S. Hochreiter, "Gans trained by a two time-scale update rule converge to a local nash equilibrium," in *Advances in Neural Information Processing Systems*, I. Guyon, U. V. Luxburg, S. Bengio, H. Wallach, R. Fergus, S. Vishwanathan, and R. Garnett, Eds., vol. 30. Curran Associates, Inc., 2017. [Online]. Available: https://proceedings.neurips.cc/paper_files/paper/2017/file/8a1d694707eb0fefe65871369074926d-Paper.pdf
- [45] A. Gretton, K. M. Borgwardt, M. J. Rasch, B. Schölkopf, and A. Smola, "A kernel two-sample test," *J. Mach. Learn. Res.*, vol. 13, no. 1, p. 723–773, Mar. 2012.
- [46] S. Zhang, T. Yu, B. Choi, F. Ouyang, and Z. Ding, "Radiomap inpainting for restricted areas based on propagation priority and depth map," *IEEE Transactions on Wireless Communications*, vol. 23, no. 8, pp. 9330–9344, 2024.

- [47] Altair, *Altair WinProp 2021 Documentation*, Altair, Troy, Michigan, USA, 2021, Accessed: 2024-12-02. [Online]. Available: <https://2021.help.altair.com/2021/winprop/index.htm>
- [48] OpenStreetMap Contributor Terms, “OpenStreetMap,” <https://www.openstreetmap.org/>, 2024.